Available online at www.sciencedirect.com

jmr&t
Journal of Materials Research and Technology
www.jmrt.com.br

Original Article

Aqueous chemical route synthesis and the effect of calcination temperature on the structural and optical properties of ZnO nanoparticles

*Mohammad Ramzan Parra, Fozia Z. Haque**

Department of Physics, Optical Nanomaterials Lab, M.A.N.I.T., Bhopal, India

ARTICLE INFO

Article history:
Received 3 April 2014
Accepted 28 July 2014
Available online 16 September 2014

Keywords:
ZnO nanoparticles
Aqueous chemical route
Average crystallite size
Scherrer's equation
Williamson–Hall method

ABSTRACT

This article reports the controlled size of ZnO nanoparticles synthesized via simple aqueous chemical route without the involvement of any capping agent. The effect of different calcination temperatures on the size of the ZnO nanoparticles was investigated. X-ray diffraction (XRD) results indicated that all the samples have crystalline wurtzite phase, and peak broadening analysis was used to evaluate the average crystallite size and lattice strain using Scherrer's equation and Williamson–Hall (W–H) method. Morphology and elemental compositions were investigated using atomic force microscopy (AFM) and scanning electron microscopy (SEM) with energy-dispersive X-ray (EDX) spectroscopy. The average crystallite size of ZnO nanoparticles estimated from Scherrer's formula and W–H analysis was found to increase with the increase in calcination temperature. These results were in good agreement with AFM results. Optical properties were investigated using UV–vis spectroscopy in diffused reflectance (DR) mode, with a sharp increase in reflectivity at 375 nm and the material has a strong reflective characteristic after 420 nm at 500 °C calcination temperature. Furthermore, photoluminescence spectroscopic results revealed intensive ultraviolet (UV) emission with reduced defect concentrations and a slight shifting in band gap energies with increased calcination temperature from 200 °C to 500 °C. This study suggests that the as-prepared ZnO nanoparticles with bandgap tunability might be utilized as window layer in optoelectronic devices.

1. Introduction

Semiconductor nanoparticles have drawn considerable interest in recent years because of their special properties such as large surface-to-volume ratio, special electronic properties and unique optical properties as compared to their bulk counterparts [1]. The large surface to volume ratio can contribute to some of the unique properties of nanoparticles. The oxides of transition metals are an important class of semiconductors [2–5]. Among various semiconducting oxides, zinc oxide (ZnO) is a distinctive electronic and photonic wurtzite n-type semiconductor with a direct band gap of 3.37 eV and a high exciton binding energy (60 meV) at room temperature [6–10]. The high exciton binding energy of ZnO would allow for excitonic

* *Corresponding author.*
E-mail: foziazia@rediffmail.com (F.Z. Haque).

http://dx.doi.org/10.1016/j.jmrt.2014.07.001
2238-7854/

transitions even at room temperature, which could mean high radiative recombination efficiency for spontaneous emission as well as a lower threshold voltage for laser emission [11,12]. The lack of center of symmetry in wurtzite, combined with a large electromechanical coupling, results in strong piezoelectric and pyroelectric properties and hence the use of ZnO in mechanical actuators and piezoelectric sensors [13]. ZnO is a potential candidate for optoelectronic applications in the short wavelength range (green, blue and ultraviolet), information storage, and sensors as it exhibits similar properties to GaN [14,15]. ZnO nanoparticles are promising candidates for various applications, such as nanogenerators, gas sensors, solar cells, photodetectors and photocatalysts [6,13,16–18].

Recently, many works have been directed to investigate the optical and electrical properties of ZnO nanomaterials, synthesized by different chemical and physical methods including vapor condensation, hydrothermal method, solution combustion method, sol–gel, etc. [19–22]. Most of these techniques have not been extensively used on a large scale, but chemical synthesis techniques have been widely used due to their simplicity and low cost. Chemical route method is one of the best methods for synthesizing material with high purity, controlled nanostructures and surface properties [23,24]. These synthesis techniques are attractive for several reasons: they are low cost, less hazardous, and thus capable of easy scaling up; growth occurs at a relatively low temperature, compatible with flexible organic substrates; there is no need for the use of metal catalysts, and thus it can be integrated with well-developed silicon technologies. In addition, there are a variety of parameters that can be tuned, to effectively control the morphologies and physical properties of the final products. Wet chemical methods have been demonstrated as a very powerful and versatile technique for growing ZnO nanoparticles.

In the present work, ZnO nanoparticles have been synthesized via simple aqueous chemical route with controlled parameters, without the involvement of any capping agent. A comparative evaluation of average crystallite size of ZnO nanoparticles obtained from direct AFM measurements and powder X-ray diffraction (XRD) peak broadening is reported. The average crystallite size and strain associated with ZnO samples due to lattice deformation have also been estimated through Williamson–Hall method. The morphology with average diameter and crystallite size of the samples were investigated using AFM and SEM, followed by the optical study using UV–vis and photoluminescence spectroscopy.

2. Experimental details

2.1. *Synthesis of ZnO nanoparticles*

For the synthesis of ZnO nanoparticles all chemical reagents used in the experiment were of analytical grade [Merck with 99% purity] without further purification. Zinc acetate dihydrate [$Zn(CH_3COO)_2{\cdot}2H_2O$], and 0.3 M sodium hydroxide (NaOH) were involved in the reaction as precursor material and pH controller. Initially [$Zn(CH_3COO)_2{\cdot}2H_2O$] was dissolved in 75 ml distilled water (DI) under constant stirring for 15 min at 60 °C. In the next step, aqueous solution of NaOH was added drop-wise for 10 min to the reaction mixture under constant stirring until the pH of the solution reached to 8. During that

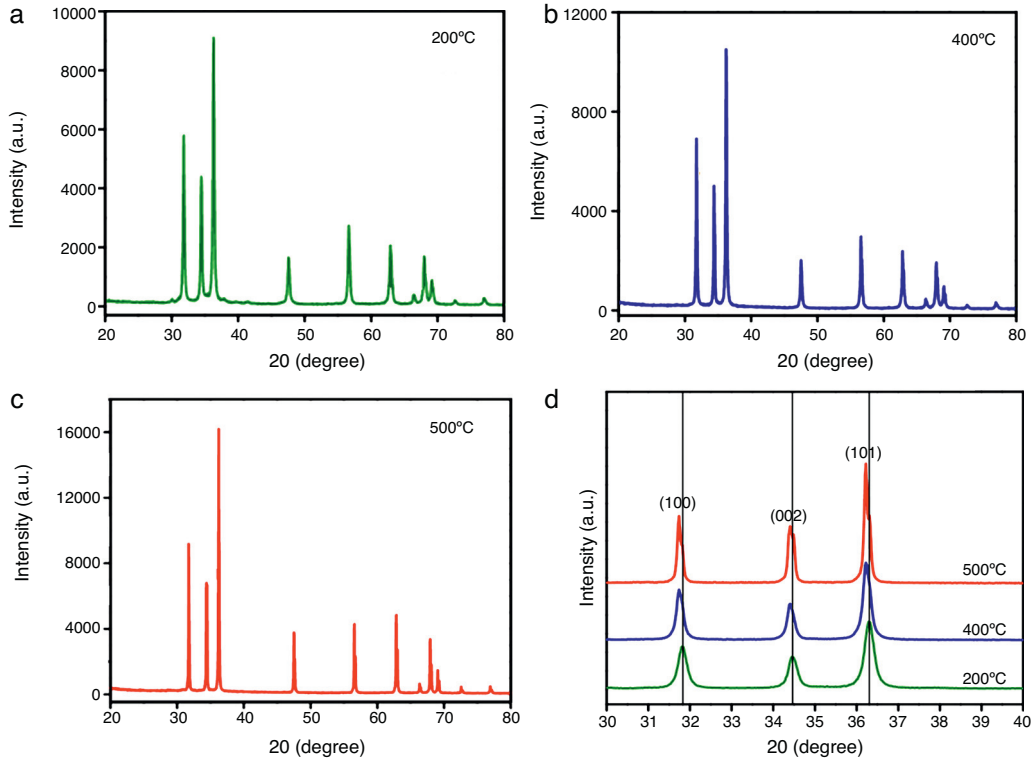

Fig. 1 – Powder X-ray diffraction patterns of ZnO nanoparticles at different calcination temperatures: (a) 200 °C, (b) 400 °C and (c) 500 °C; (d) shifting in peaks position.

process, a white precipitate was formed in the solution. After 7 h, the reaction mixture was centrifuged to get the precipitate out and washed several times with deionized (DI) water and ethanol. Finally, nanocrystalline ZnO powders with a milky white color were obtained after calcination at 200 °C, 400 °C and 500 °C for 3 h in muffle furnace.

2.2. *Characterizations*

Powder X-ray diffraction data of the ZnO nanoparticles was collected in Bruker D8 Advance X-ray diffractrometer. Diffraction peaks were compared with those of the standard compounds reported in the JCPDS files (80-0075 card ICSD#: 067849). Morphology and elemental compositions were investigated using scanning electron microscopy (SEM, JEOL-JSM-6390, operating at 10 kV) with energy-dispersive X-ray (EDX) spectroscopy and atomic force microscopy (AFM) NT-MDT Solver NEXT. Band gap energies were observed using UV–vis-NIR spectrometer (Perkin Elmer Lambda 950) in diffuse reflectance mode and emission spectra were observed by photoluminescence spectroscopy (F-7000, Hitachi) with excitation wavelength (λ_{ex}) = 325 nm using xenon lamp as source unit operated at room temperature.

3. Results and discussion

3.1. *X-ray diffraction analysis of ZnO nanoparticles*

The effect of different calcination temperatures on the ZnO nanoparticles are shown in Fig. 1. All the peaks were sharpened at a temperature greater than 200 °C, which confirm the growth of crystals at higher calcination temperatures. It is clear from Fig. 1 that except hexagonal phase of ZnO no other phase was developed. The recorded X-ray diffraction patterns were compared with the standard ZnO pattern (JCPDS: 80-0075 card ICSD#: 067849). ZnO nanoparticles calcined at higher temperature shift in peak positions (1 0 0), (0 0 2) and (1 0 1) towards the lower Bragg's angle as compared to lower calcination temperature. Fig. 1d illustrates a gradual shifting in peak positions of the samples.

The crystallite size of the ZnO nanoparticles was calculated by the X-ray line broadening method using the Scherrer's equation:

$$D = \frac{K\lambda}{\beta_{hkl}\cos\theta} \quad (1)$$

where D is the crystallite size, λ the Cu K_α radiation of wavelength (1.5406 Å), K the shape factor (0.9), β_{hkl} is the full width at half maximum (FWHM) in radian and θ is the scattering angle. From the calculations, the average crystallite size of the ZnO nanoparticles was in the range from 30 nm to 44 nm, as shown in Table 1.

3.2. *Williamson–Hall analysis*

Williamson–Hall X-ray line broadening analysis provides a method of finding an average size of coherently diffracting domains and strain. Strain induced peak broadening arises due to crystal imperfection; and distortion, which had been calculated using the relation:

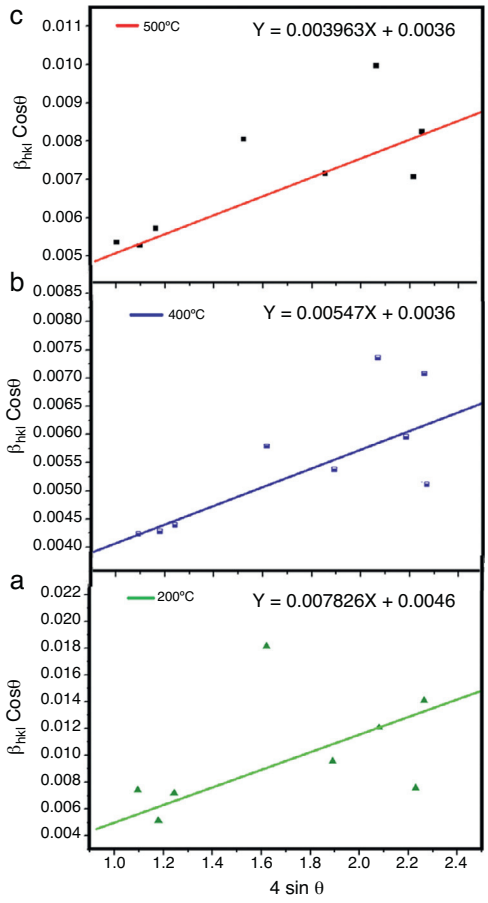

Fig. 2 – Williamson–Hall analyses of ZnO nanoparticles calcined at (a) 200 °C, (b) 400 °C and (c) 500 °C temperatures assuming UDM plot.

$$\varepsilon = \frac{\beta_{hkl}}{4\tan\theta} \quad (2)$$

To estimate microstrain from the X-ray diffraction pattern Williamson and Hall [25] proposed a modified Scherrer's formula as:

$$\beta_{hkl}\cos\theta = \frac{K\lambda}{D} + 4\varepsilon\sin\theta \quad (3)$$

Eq. (3) represents the linear plot of $\beta_{hkl}\cos\theta$ against $4\sin\theta$ for the samples calcined at 200 °C, 400 °C and 500 °C temperatures displayed in Fig. 2. The slope of the plots provides the values of strain (ε) which are 0.0078, 0.0054 and 0.0039 respectively. The results were reasonable with the crystallite sizes obtained from the XRD (Scherrer's formula) where small ε give rise to large crystallite size. Large ε caused small crystallite size associated with small grain size. It was observed from the calculations that with the increase in calcination temperature from 200 °C to 500 °C, the strain associated with the samples decreased with a gradual increase in crystallite size, as shown in Table 1.

Table 1 – Comparison of the geometric parameters of ZnO nanoparticles obtained from Scherrer's formula, W–H analysis and AFM results.

Sample	Calcination temperature (°C)	Average crystallite size, D (nm)			
		Scherrer's D (nm)	Williamson–Hall analysis		AFM analysis (nm)
			D (nm)	ε	
a	200	30	49	0.0078	28
b	400	41	68	0.0054	39
c	500	44	72	0.0039	44

3.3. *Morphological analysis*

Surface morphology was determined through AFM and corresponding SEM images of the samples, as shown in Fig. 3 and Fig. 4a. From the AFM images, the crystallite size of the samples was found in nanometer range. As the calcination temperature increased from 200 °C to 500 °C, the crystallite sizes increased from 28 nm to 44 nm. With the increase in the calcination temperature, the nucleation rate of the particles increased more rapidly. This is due to the increase in supersaturation of the reaction products, which accelerated the crystal core forming reaction within a short time. Under these conditions, the controlling step of the reaction is transferred from grain growth to crystal nucleus formation. With the temperature continuing to rise, the phenomenon of "nuclear-aggregation" caused by the rapid formation of crystal nucleus is obvious, which results in aggregation among the crystal nucleus. The rate of particle aggregation is a major factor that controls the morphology and structure (crystalline) of the final products. It was determined that larger grain samples were inherently more rough due to the increased differences in height (Z range) at their boundaries as compared to the smaller grains. However, the morphologies were quite similar in all cases. A similar conclusion can be drawn from the SEM observation. It was found that the morphology markedly depend on the process parameters.

Table 1 summarizes the geometric parameters of ZnO nanoparticles obtained from Scherrer's formula, W–H analysis, and AFM results. By comparing the values of average crystallite size obtained from W–H analysis, it was found that, the inclusion of strain has a very small effect on the average crystallite size of ZnO nanoparticles. However, the average crystallite size obtained from Scherrer's formula and W–H analysis showed a small variation; this variation was

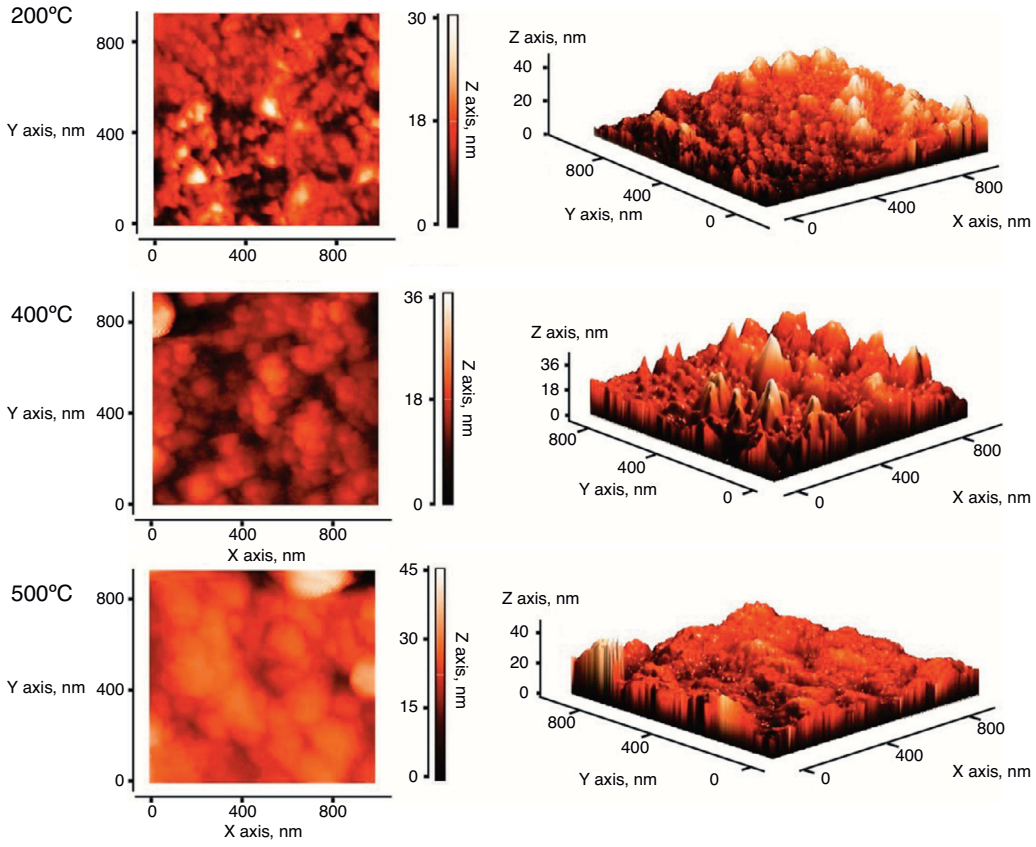

Fig. 3 – Two-dimensional and three-dimensional atomic force microscopic phase diagram of ZnO nanoparticles calcined at (a) 200 °C, (b) 400 °C and (c) 500 °C.

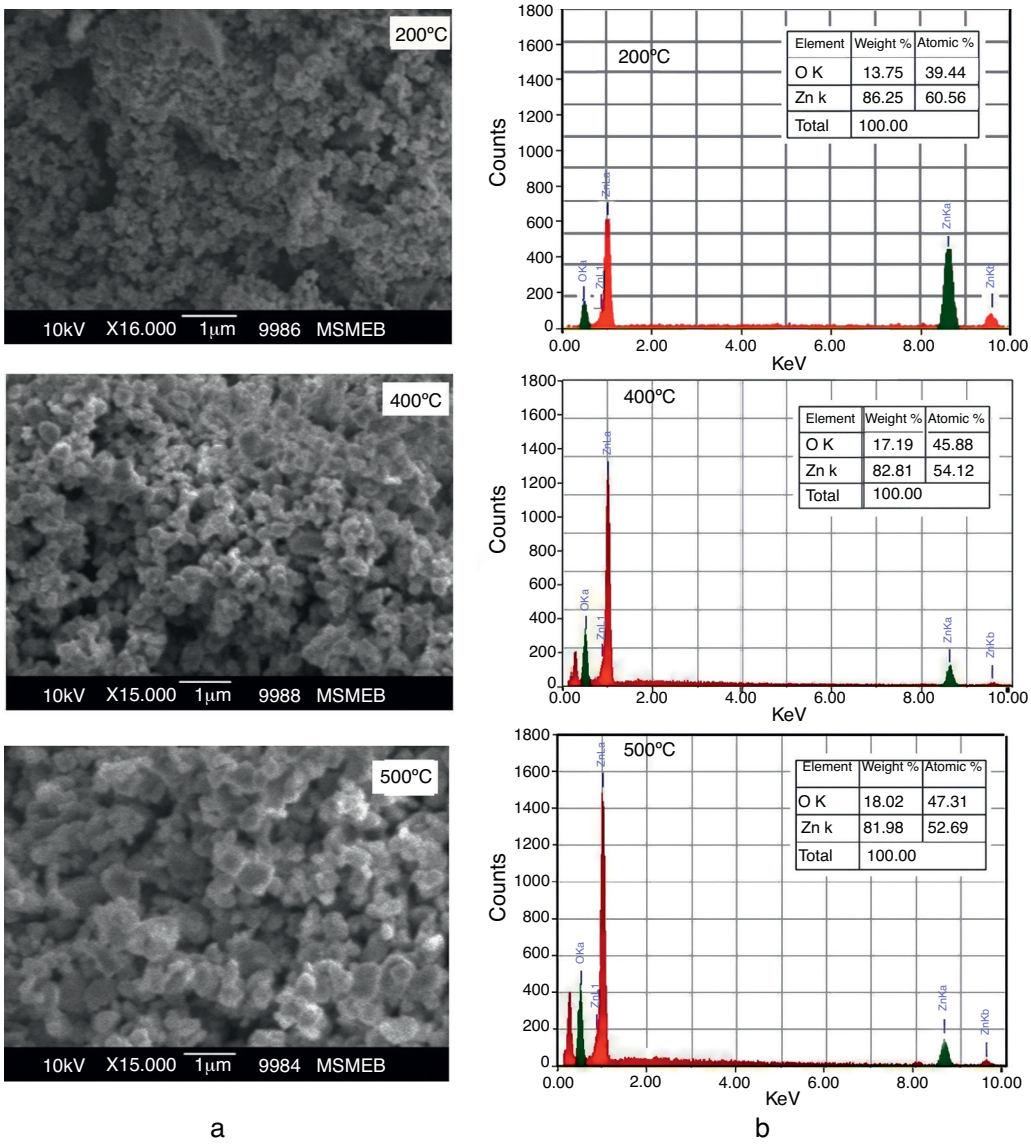

Fig. 4 – (a) Scanning electron microscopic images of ZnO nanoparticles calcined at 200 °C, 400 °C and 500 °C. (b) Energy-dispersive analysis X-ray (EDAX) images of the as-prepared ZnO nanoparticles calcined at 200 °C, 400 °C and 500 °C.

because of the difference in averaging the particle size distribution.

The elemental compositions of the ZnO nanoparticles were observed using energy dispersive X-ray spectroscopy. The EDX data show almost the same peaks for all samples. Fig. 4b represents EDX patterns which indicate that the as prepared ZnO nanoparticles were composed of only Zn and O. No evidence of other impurities was found and the ZnO nanoparticles were nearly stoichiometric. This observation was in good agreement with XRD results, which confirmed the phase purity of ZnO nanoparticles.

3.4. *Optical study*

3.4.1. *UV–vis analysis*

The effect of different calcination temperatures on the optical properties of ZnO nanoparticles were investigated and are shown in Fig. 5. The diffused reflectance spectra showed a sharp increase at 375 nm and the material had a strong reflective characteristic after approximately 420 nm for the sample calcined at 500 °C. This was due to the high possibility of reflectance for the photons lacking the required energy for interacting with electrons or atoms. It was observed that the absorption of the ZnO nanoparticles was strongly affected by the particle sizes. The band gap energies were determined using Kubelka–Munk function:

$$F(R) = \frac{(1-R)^2}{2R} \tag{4}$$

Here (R) is the absolute value of reflectance and $F(R)$ is equivalent to the absorption coefficient. The direct band gap of ZnO was estimated by plotting $[F(R)\cdot h\nu]^2$ vs. $h\nu$ (eV). The linear part of the Tauc plot was extrapolated to $[F(R)\cdot h\nu]^2 = 0$ to get the direct band gap energy. The obtained bandgap energy

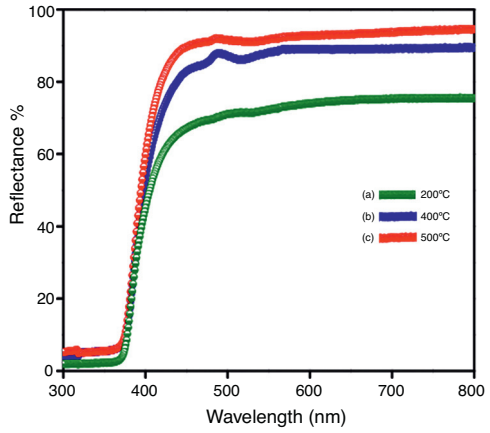

Fig. 5 – Diffuse reflectance spectra of the ZnO nanoparticles calcined at 200 °C, 400 °C and 500 °C temperatures.

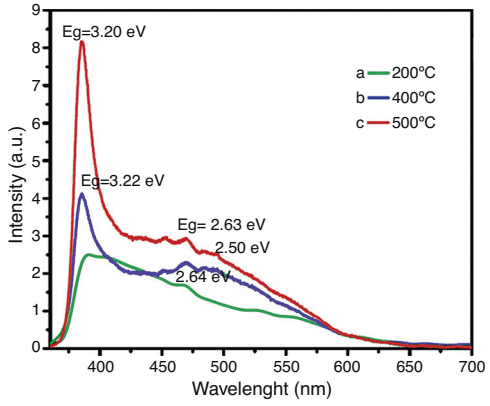

Fig. 6 – Photoluminescence emission spectra of ZnO nanoparticles calcined at 200 °C, 400 °C and 500 °C.

(E_g) values were 3.23, 3.22 and 3.20 eV as the temperature increased from 200 °C to 500 °C respectively. Compared to the reported values of bandgap energy of bulk ZnO (E_g = 3.37 eV) [6], the optical absorption edge slightly shifted toward longer wavelength, which may be attributed to the increase in grain size at higher calcination temperatures [26].

3.4.2. *Photoluminescence analysis*

PL spectra of all the samples mainly consist of three emission bands as shown in Fig. 6, a strong UV emission band at 3.2 eV, a very weak violet band at 2.97 eV, and a week blue band at 2.60 eV. The strong UV emission corresponds to the exciton recombination related near-band edge (NBE) emission of ZnO. The violet emission band is due to the recombination of an electron at the zinc interstitial (Z_{in}) and a hole in the valance band [27,28]. The weak blue emission corresponds to the electron transition from the conduction band to interstitial oxygen defects (O_{in}) in the ZnO. The intensity ratio between the near-band-edge UV emission and the visible region is usually used to evaluate the quality of ZnO. Photoluminescence results revealed that the ultraviolet emission peak of the samples calcined at higher temperature become sharp and narrow with high intensities as compared to visible emission peak. These results essentially agree with the analysis, which results in the shift of the optical absorption edge presented above. Thus, the red shift of the optical bandgap and improved ultraviolet emission at higher calcination temperature improved crystallinity and reduced defect concentrations in ZnO samples.

4. Conclusion

ZnO nanoparticles with average crystallite size of 28–44 nm were successfully synthesized via aqueous chemical route. The effect of different calcination temperatures on the structural and optical properties was investigated. The XRD results indicated that all the samples have pure wurtzite ZnO phase with well crystallinity. It was observed from the calculations that with the increase in calcination temperature from 200 °C to 500 °C, the strain associated with the samples decreased with a gradual increase in crystallite size. The average crystallite size obtained from AFM analysis were in good agreement with the results obtained from Scherrer formula based on X-ray diffraction analysis. Red shifting in band gap energies from E_g = 3.23 eV to 3.20 eV with intensive ultraviolet (UV) emission was observed with increasing calcination temperature from 200 °C to 500 °C.

Conflicts of interest

The authors declare no conflicts of interest.

Acknowledgments

The authors would like to thank Director, UGC-DAE-CSR Indore center, India for UV-vis and XRD characterizations.

REFERENCES

[1] Abou El-Nour KMM, Eftaiha A, Al-Warthan A, Ammar RAA. Synthesis and applications of silver nanoparticles. Arab J Chem 2010;3:135–40.
[2] Nirmala JNS, Sagayaraj P. The influence of capping by TGA and PVP in modifying the structural, morphological, optical and thermal properties of ZnS nanoparticles. Appl Sci Res 2012;4(2):1079–90.
[3] Alabi AB, Coppede N, Vilani M, Calestani D, Zappetini A, Babalola O, et al. Photocatalytic activity of nanostructured copper (II) oxide particles. Ife J Sci 2013;15(2):409–14.
[4] Rao CNR, Rao GVS. Transition metal oxide, crystal chemistry phase transition and related aspects, NSRDS-NBS 49. Washington DC: U.S. Government Printing Office; 1974.
[5] Mark TG, Zheng HL. Thin-film metal oxides in organic semiconductor devices: their electronic structures, work functions and interfaces. NPG Asia Mater 2013;5:e55, http://dx.doi.org/10.1038/am.2013.29.
[6] Li D, Hu J, Fan F, Bai S, Luo R, Chen A, et al. Quantum-sized ZnO nanoparticles synthesized in aqueous medium for toxic gases detection. J Alloys Compd 2012;539:205–9.
[7] Rajeswari YN, Srinivasan R, Chandra BA. Multi-capping agents in size confinement of ZnO nanostructured particles. Opt Mater 2009;31:1570–4.

[8] Kumbhakar P, Singh D, Tiwary CS, Mitra AK. Chemical synthesis and visible photoluminescence emission from monodispersed ZnO nanoparticles. Chalcogenide Lett 2008;5(12):387–94.
[9] Al-Heniti S, Badran RI, Umar A, Al-Ghamdi A, Kim SH, Al-Marzouki F, et al. Temperature dependant structural and electrical properties of ZnO nanowire networks. J Nanosci Nanotechnol 2011;11:1–7.
[10] Wang ZH, Geng DY, Han Z, Zhang ZD. Characterization and optical properties of ZnO nanoparticles obtained by oxidation of Zn nanoparticles. Mater Lett 2009;63: 2533–5.
[11] Samuel SM, Bose L, George KC. Optical properties of ZnO nanoparticles. SB Acad Rev 2009;1(2):57–65.
[12] Karami H, Fakoori E. Synthesis and characterization of ZnO nanorods based on a new gel pyrolysis method. J Nanomater 2011, http://dx.doi.org/10.1155/2011/628203 [Article ID 628203; 11 pp.].
[13] Xudong W, Jinhui S, Zhong LW. Nanowire and nanobelt arrays of zinc oxide from synthesis to properties and to novel devices. J Mater Chem 2007;17:711–20.
[14] Lupan O, Pauporte T, Chow L, Viana B, Pelle F, Ono LK, et al. Effects of annealing on properties of ZnO thin films prepared by electrochemical deposition in chloride medium. Appl Surf Sci 2010;256:1895–907.
[15] Chen R, Zou C, Yan X, Alyamani A, Gao W. Growth mechanism of ZnO nanostructures in wet-oxidation process. Thin Solid Films 2011;519:1837–44.
[16] Ma Y, Wang WL, Liao KJ, Kong CY. Study on sensitivity of nano-grain ZnO gas sensors. J Wide Bandgap Mater 2002;10:113–20.
[17] Ali AA, Azam IZ, Seyed MM, Mohammad MA. Photocatalytic activity of ZnO nanoparticles prepared via submerged arc discharge method. Appl Phys A 2010;100: 1097–102.
[18] Waldo JEB, Martijn MW, Martijn K, Xiaoniu Y, René AJJ. Hybrid zinc oxide conjugated polymer bulk heterojunction solar cells. J Phys Chem B 2005;109:9505–16.
[19] Zhong LW, Jinhui S. Piezoelectric nanogenerators based on zinc oxide nanowire arrays. Sci Mag 2006;312:242–6.
[20] Mohammad AA, Mahmudur RI, Quayum ME. Fabrication of ZnO nanoparticles by solution combustion method for the photocatalytic degradation of organic dye. J Nanostruct Chem 2013;3(36).
[21] Urgessa ZN, Oluwafemi OS, Botha JR. Hydrothermal synthesis of ZnO thin-films and its electrical characterization. Mater Lett 2012;79:266–9, http://dx.doi.org/10.1016/j.matlet.2012.04.065.
[22] Singh N, Pandey P, Haque FZ. Effect of heat and time-period on the growth of ZnO nanorods by sol–gel technique. Optik 2012;123:1340–2.
[23] Pandey P, Singh N, Haque FZ. Development and optical study of hexagonal multi-linked ZnO micro-rods grown using hexamine as capping agent. Optik 2013;124:1188–2119.
[24] Singh AK, Viswanath V, Janu VC. Synthesis, effect of capping agents, structural, optical and photoluminescence properties of ZnO nanoparticles. J Lumin 2009;129:874–8.
[25] Zak AK, Majid WHA, Abrishami ME, Yousefi R. X-ray analysis of ZnO nanoparticles by Williamson Hall and size strain plot methods. Solid State Sci 2011;13:251–6.
[26] Babu KS, Reddy AR, Sujatha C, Reddy VK, Mallika AN. Synthesis and optical characterization of porous ZnO. J Adv Ceram 2013;2(3):260–5.
[27] Haque FZ, Singh N, Pandey P, Parra MR. Study of zinc oxide nano/micro rods grown on ITO and glass substrates. Optik 2013;124(20):4167–71.
[28] Parra MR, Haque FZ. Structural and optical properties of poly-vinylpyrrolidone modified ZnO nanorods synthesized through simple hydrothermal process. Optik 2014;(17): 4629–32, http://dx.doi.org/10.1016/j.ijleo.2014.05.030.